ANALYSIS AND MODELING OF SHEAR WAVES GENERATED BY EXPLOSIONS AT THE SAN ANDREAS FAULT OBSERVATORY AT DEPTH

Fred F. Pollitz, William L. Ellsworth, and Justin L. Rubinstein

US Geological Survey, Menlo Park, CA

Sponsored by the National Nuclear Security Administration

Award No. DE-AI52-09NA29328
Proposal No. BAA09-69

ABSTRACT

Using a deep deployment of an 80-element, 3-component borehole seismic array stretching from 1.5 to 2.3 kilometer (km) depth at the San Andreas Fault Observatory at Depth (SAFOD), we examine recordings of chemical explosions to better understand the generation of shear waves by explosive sources. The well is near-vertical at 1.5km and gradually transitions to a dip of 38 degrees at the deepest recording location. The chemical shots are high velocity chemical shots buried between 10-30 m and fired electrically, of size ~36 kg. The shotpoints are offset from the wellhead by 1 to 2 km. Previous analysis of zero-offset recordings (Pollitz et al., 2012) gave a velocity structure ranging from 1500 m/s (meters per second) in the upper 50 meters to 5000 m/s at the bottom of the well, as well as attenuation structure. The larger-offset recordings analyzed here have a strong, impulsive P arrival polarized as a longitudinal wave, and S waves composed of dominantly converted P to SV at the internal discontinuities and, to a lesser extent, the upward P to downgoing S converted wave pS.

We compute synthetic waveforms using the Direct Radial Integration method of Friederich and Dalkolmo (1995), which handles a layered transversely isotropic medium with anelasticity. We use a hybrid 1D structure consisting of the local Bleibinhaus et al. (2007) structure determined from an active-source experiment combined with the near-well structure determined from the zero-offset shots. Using forward modeling on this velocity structure, both observed P and S wave energy are identified with the traveltimes expected for direct and/or reflected phases as well as the moveout associated with the local velocity structure around the receiver array. For larger-offset shots, S-wave energy is polarized primarily along the radial and propagation direction, consistent with converted P to SV energy. The longer-offset shots analyzed here have more distinct and energetic S arrivals than seen for the zero-offset shots, likely because of greater P to S conversions along the longer propagation paths. Forward modeling using the synthetics enables a reasonable match to observed arrival times and moveouts of major body-wave packets and suggest an additional vertical-dipole source, which represents damage.

Seismic data from the Hole-Ryberg Line, a 46 km long refraction line, further illuminates sources of S wave energy. Three-component recordings obtained from a line of 100 kg chemical shots detonated along the line reveal substantial SV and SH energy, tending to increase with distance from the source. The line crosses several geologic boundaries with substantial lateral variations in seismic velocity (e.g. McPhee et al., 2004). The generated S energy is interpreted to arise from P to S conversions at subhorizontal discontinuities, and the generated SH energy from P to S conversions at near-vertical discontinuities and/or scatterers away from the vertical plane containing the direct raypath.

Report Documentation Page

Form Approved
OMB No. 0704-0188

1. REPORT DATE	2. REPORT TYPE	3. DATES COVERED
SEP 2012		**00-00-2012 to 00-00-2012**

4. TITLE AND SUBTITLE	5a. CONTRACT NUMBER
Analysis and Modeling of the Shear Waves Generated by Explosions at the San Andreas Fault Observatory at Depth	5b. GRANT NUMBER
	5c. PROGRAM ELEMENT NUMBER
6. AUTHOR(S)	5d. PROJECT NUMBER
	5e. TASK NUMBER
	5f. WORK UNIT NUMBER
7. PERFORMING ORGANIZATION NAME(S) AND ADDRESS(ES) **US Geological Survey, Menlo Park,345 Middlefield Rd,Menlo Park,CA,94025**	8. PERFORMING ORGANIZATION REPORT NUMBER
9. SPONSORING/MONITORING AGENCY NAME(S) AND ADDRESS(ES)	10. SPONSOR/MONITOR'S ACRONYM(S)
	11. SPONSOR/MONITOR'S REPORT NUMBER(S)

12. DISTRIBUTION/AVAILABILITY STATEMENT
Approved for public release; distribution unlimited

13. SUPPLEMENTARY NOTES
Published in the Proceedings of the 2012 Monitoring Research Review - Ground-Based Nuclear Explosion Monitoring Technologies, 18-20 September 2012, Albuquerque, NM. Volume I. Sponsored by the Air Force Research Laboratory (AFRL) and the National Nuclear Security Administration (NNSA).

14. ABSTRACT

Using a deep deployment of an 80-element, 3-component borehole seismic array stretching from 1.5 to 2.3 kilometer (km) depth at the San Andreas Fault Observatory at Depth (SAFOD), we examine recordings of chemical explosions to better understand the generation of shear waves by explosive sources. The well is near-vertical at 1.5km and gradually transitions to a dip of 38 degrees at the deepest recording location. The chemical shots are high velocity chemical shots buried between 10-30 m and fired electrically, of size ~36 kg. The shotpoints are offset from the wellhead by 1 to 2 km. Previous analysis of zero-offset recordings (Pollitz et al., 2012) gave a velocity structure ranging from 1500 m/s (meters per second) in the upper 50 meters to 5000 m/s at the bottom of the well, as well as attenuation structure. The larger-offset recordings analyzed here have a strong, impulsive P arrival polarized as a longitudinal wave, and S waves composed of dominantly converted P to SV at the internal discontinuities and, to a lesser extent, the upward P to downgoing S converted wave pS. We compute synthetic waveforms using the Direct Radial Integration method of Friederich and Dalkolmo (1995) which handles a layered transversely isotropic medium with anelasticity. We use a hybrid 1D structure consisting of the local Bleibinhaus et al. (2007) structure determined from an active-source experiment combined with the nearwell structure determined from the zero-offset shots. Using forward modeling on this velocity structure, both observed P and S wave energy are identified with the traveltimes expected for direct and/or reflected phases as well as the moveout associated with the local velocity structure around the receiver array. For larger-offset shots, S-wave energy is polarized primarily along the radial and propagation direction, consistent with converted P to SV energy. The longer-offset shots analyzed here have more distinct and energetic S arrivals than seen for the zero-offset shots likely because of greater P to S conversions along the longer propagation paths. Forward modeling using the synthetics enables a reasonable match to observed arrival times and moveouts of major body-wave packets and suggest an additional vertical-dipole source, which represents damage. Seismic data from the Hole-Ryberg Line, a 46 km long refraction line, further illuminates sources of S wave energy. Three-component recordings obtained from a line of 100 kg chemical shots detonated along the line reveal substantial SV and SH energy, tending to increase with distance from the source. The line crosses several geologic boundaries with substantial lateral variations in seismic velocity (e.g. McPhee et al., 2004). The generated S energy

15. SUBJECT TERMS

16. SECURITY CLASSIFICATION OF:			17. LIMITATION OF ABSTRACT	18. NUMBER OF PAGES	19a. NAME OF RESPONSIBLE PERSON
a. REPORT	b. ABSTRACT	c. THIS PAGE			
unclassified	**unclassified**	**unclassified**	**Same as Report (SAR)**	**11**	

OBJECTIVES

The principal objective of the work being undertaken is to better characterize and understand the generation of S waves from explosive sources. The amplitudes of *S* waves are commonly used as a discriminant between explosion- and earthquake-generated sources, in that explosion sources primarily produce P waves. Thus, characterizing how S waves are generated by explosive sources is critical to improving explosion discrimination criteria. In this project, we focus on *S* waves generated in the near-source region (up to several km laterally and 2.5 km in depth).

RESEARCH ACCOMPLISHED

Downhole Observations

The 80-level P/GSI Main Hole Array (Paulsson Geophysical Services, Inc.) of 3-component borehole instruments (15 m spacing) was deployed between the surface and 2.3 km depth in the SAFOD Main Hole (Zoback et al., 2010) in May 2005 (Chavarria et al., 2007). More than three terabytes of continuous, high sample rate data were collected, including 14 explosions at PASO array stations (Figure 1). Each shot consisted of 36 kg of Pentolite (detonation velocity
7.8 km/s) emplaced in a vertical borehole between 20 m and 30 m depth. We focus on shots conducted at PASO stations on the southwest side of the San Andreas fault in order to avoid the substantial lateral variability in velocity structure across the SAF. Record sections for 3-component velocity recorded from shots at PIGH, BURN, and FLIP are shown in Figures 2, 3, and 4. The seismograms are resolved onto three borehole-oriented components: Axial=locally downhole; Dip=component in the vertical plane locally passing through the borehole and perpendicular to it. Strike=horizontal component locally perpendicular to the borehole. For all shots, the recordings exhibit strong P waves on the longitudinal component (primarily the axial component for the PIGH shot; primarily the strike component for the BURN and FLIP shots). Wave packets arriving with the expected S-wave moveout are seen for all shots, particularly PIGH.

Methods for Computing Synthetic Seismograms

Synthetic seismograms are generated using the Direct Green's Function (DGF) method of Friederich and Dalkolmo (1995). This method synthesizes the seismic wavefield for a spherically layered structure of seismic velocities V_p and V_s, density ρ, and attenuation factors Q_p and Q_s in the $l-\omega$ domain, where l denotes spherical harmonic degree. It is the spherical equivalent of the frequency-wavenumber method employed for flat-layered structures (e.g., Zhu and Rivera, 2002). It has been validated against analytic solutions, including those for elastic wave propagation in a full space for both isotropic and shear sources (eq. 4.29 of Aki and Richards [1980]) and in a half-space, e.g., Lamb's Problem (Kuhn, 1985), as well as the independent numerical solutions AXITRA (Bouchon, 1981) and $f-k$ method (Zhu and Rivera, 2002).

The DGF method is applied to buried sources in the layered structure given in Figure 5. The velocity structure is a hybrid of a regional 2D velocity structure determined on a profile passing close to the SAFOD well (Bleibinhaus et al., 2007) and a 1D velocity structure determined for the local SAFOD well using near-zero offset shots (Pollitz et al., 2012). The velocity structure in the upper 2.0 km is modified from a 1D model extracted from the Bleibinhaus et al. (2007) model near PIGH, while the velocity structure below 2.0 km is the local SAFOD structure. A velocity discontinuity at 0.5 km depth, not present in the Bleibinhaus et al. (2007) model, is introduced in order to partially account for waves observed to arrive mid-way between expected direct P and direct S, which are tentatively interpreted as P to S conversions at internal discontinuities. The attenuation structure is based on forward modeling trials aimed at accounting for the amplitude decay with distance and frequency content of our observations. The V_s structure is based on the V_p structure and the V_p/V_s ratio determined by regional tomography (Zhang et al., 2009), and the density structure is based on empirical $V_p-\rho$ relationships (Gardner et al., 1984; Brocher, 2006). The Q_s values are not estimated from the data but are chosen such that the quality factor for bulk modulus is twice that for shear modulus.

For a x − y − z coordinate system (where x, y, and z denote distance in the due East, North, and Up directions, respectively) and a point source located at $r_0 = (x_0, y_0, z_0)$, we consider a moment tensor density M(r) given by

$$\mathbf{M} = M_{\text{expl}} \begin{pmatrix} 1 & 0 & 0 \\ 0 & 1 & 0 \\ 0 & 0 & 1 \end{pmatrix} H(t)\delta(\mathbf{r}, \mathbf{r}_0) + M_{\text{d}} \begin{pmatrix} 0 & 0 & 0 \\ 0 & 0 & 0 \\ 0 & 0 & 1 \end{pmatrix} H(t)\delta(\mathbf{r}, \mathbf{r}_0)$$

where H(t) is the step function, δ(r,r0) is the Dirac delta function, and Mexpl and Md are the moments associated with explosion and vertical-dipole source components, respectively. This is simply the sum of two volumetric sources: a monopole explosion and a vertical dipole source representing damage (Mosse, 1981; Patton and Taylor, 2011), and it is equivalent to the sum of an explosive source and CLVD source. Although a delayed implosion likely accompanies the chemical explosions because of collapse of a cavity surrounding the source (Pollitz et al., 2012), we do not attempt to model the implosive components here.

Simulation of Explosive Sources and Their Fit to Downhole Observations

Synthetic record sections using an explosive source and corresponding to the various shots are shown in Figures 6, 7, and 8. The inclination of the borehole is 5° from vertical at 1500 m and is progressively steeper at greater depth, up to 55° at 2.3 km depth with a dip towards the northeast. Thus the axial-component velocity is dominated by vertical velocity in the upper part of the record section and includes progressively greater northeastward component with greater depth. Prominent arrivals include direct P and pS but also converted P to SV waves at internal discontinuities. The velocity discontinuity at 0.5 km depth (Figure 1) is partially effective in matching the wave packet labeled P0.5S, which we interpret as an S wave converted from downgoing P at this discontinuity. The very slow moveout at the deeper receivers (those at >2 km depth) is matched by the synthetics since the velocity model has a low-velocity zone between 2.0 and 2.5 km depth, i.e., in the lower half of the borehole array. The strong velocity discontinuity at 2.0 km depth gives rise to another converted S wave, best seen in the PIGH record and there labelled P2.0S.

Simulation of Vertical-Dipole Sources

CLVD-equivalent source components are often inferred from far-field modeling of nuclear explosions (Dreger and Woods, 2002; Patton and Taylor, 2011). Inference of vertical-dipole source components here is tentative and based on matching the temporal spread of wave packets arriving relatively late with the S wave moveout. For example, the synthetic PIGH shot record section using a purely explosive source (Figure 6) predicts only a pS arrival, which coincides with an observed arrival on the dip component (Figure 2) but does not capture observed S wave arrivals in the ~0.10 – 0.15 s before the pS wave (Figure 2). We performed trial-and-error modeling designed to broaden the temporal spread of late-arriving S energy, which likely represents a combination of direct S, direct S multiples from shallow discontinuities, and pS. For the PIGH record, the synthetics calculated using a model of the source using a ratio Md/Mexpl=0.7 (Figure 9) produces a better match to these S wave arrivals than those calculated using a purely explosive source Md/Mexpl=0 (Figure 6).

S wave energy arriving about 0.15 s before the time expected for pS is also seen on the BURN record section (Figure 3). Forward modeling of combined explosive and vertical-dipole sources as described above confirms that a vertical-dipole source produces additional S-wave energy preceding pS. However, in general, it is difficult to replicate the full extent of observed S wave energy arriving between the time of P0.5S (i.e., the P to S conversion at the 0.5 km deep discontinuity) and pS. This and the greater observed broadness of the observed P0.5S wavetrain -- relative to the synthetic P0.5S wavetrains -- suggests that both P-wave and S-wave multiples from very shallow discontinuities contribute to the broadness of a number of major observed seismic phases. Such multiples were previously modeled for the near-zero offset shots using a velocity model with a strong low-velocity zone in the upper 50 m (Pollitz et al., 2012).

Observations along the Hole-Ryberg Line

A refraction survey was conducted along a 46 km long refraction line (Figure 10) in November 2003 for purposes of regional velocity characterization in preparation for the SAFOD experiment Hole et al., 2006). Sixty-three shots were detonated along the line with a shot size of 100 kg at nominal 1 km spacing along the line (and 25 kg within a denser portion near the SAF). These shots were recorded by an array of surface seismometers, used by Hole et al. (2006) and Bleibinhaus et al. (2007) to estimate local velocity structure, as well as the 32-level 3C SAFOD Pilot

Hole array (Oye and Ellsworth, 2005). Sensors are placed at 40 m intervals between 856 and 2096 m below ground level. Recordings on the Pilot Hole array are useful for constraining the properties of the wavefield at distances up to ~20 km from the explosive source.

Shot gathers at level 10 of the receiver array (1.74 km below ground level) from shots to the northeast and southwest of the Pilot Hole are shown in Figures 11 and 12, respectively. All shot gathers exhibit clear P-wave arrivals on the vertical and radial components. The shot gather on the southwest side exhibits large-amplitude later arrivals traveling at the S wave speed on the vertical and transverse components, corresponding to SV and SH waves, respectively. The SV arrivals are likely associated with P to S conversions at subhorizontal discontinuities at depths between the surface and 1.74 km depth, while the SH arrivals are likely associated with P to S conversions at subvertical discontinuities or isolated scatterers located away from the vertical plane containing the source and receiver. The large size of these shots may make them capable of producing significant secondary source components (e.g., vertical-dipole source components) as found for recordings of nuclear tests (Patton and Taylor, 2011). The precise origins of the S wave energy may be clarified by future 2D and 3D forward modeling of the seismic wavefield through velocity structures available for the region (Hole et al., 2006; Bleibinhaus et al., 2007; Zhang et al., 2009). These velocity structures involve several subhorizontal and vertical discontinuities (e.g., at the SAF) and are likely to account for at least part of the generated S wave energy.

Discussion

All borehole records exhibit considerable wave energy arriving about mid-way between the direct P and direct S arrivals (Figures 2, 3, and 4). These wave packets arrive with the S wave moveout and are likely incident as downgoing S from the top of the receiver array ~ 1.5 km depth at a minimum. If the velocity structure varied only with depth, then these observations would demand P to S conversions at horizontal discontinuities between the surface and 1.5 km depth. Our velocity model accommodates this with a discontinuity at 0.5 km depth (Figure 5). However, the waves observed on the transverse component are much stronger than predicted, i.e., the strike component for the PIGH shot (Figure 2) or the axial component for the BURN and FLIP shots (Figures 3 and 4). This suggests that some of the converted P to S waves must be on sub-vertical discontinuities and/or other scatterers located off the direct source-receiver path.

While a single 1D velocity model enables approximate matches of synthetics to the arrival times and moveouts of several observed seismic phases, it is deficient in several details. The amplitude of synthetic pS is always greater than that of observed pS, which is present in the observed PIGH section (Figure 2) but barely discernable in the BURN and FLIP sections (Figures 2 and 3). It is possible that observed pS is weaker than predicted because of secondary shear in a small volume above the source, as was inferred to be the case for a small-offset shot that produced a substantial observed pS wave (Pollitz et al., 2012). The moveouts of all identified seismic phases for the synthetic FLIP section (Figure 8) are flatter than observed (Figure 4). This is likely because of the strong lateral velocity gradient near the SAFOD well, becoming slower as the deeper borehole approaches the SAF (Hole et al., 2006; Bleibinhaus et al., 2007; Zhang et al., 2009). Thus all propagating waves are likely sampling progressively lower-velocity material on the paths to the deeper borehole stations, resulting in a steeper moveout than predicted by the 1D model, which does not account for such lateral variations.

CONCLUSIONS AND RECOMMENDATIONS

Downhole recordings of near-surface chemical explosions at offsets of a few kilometers from the SAFOD Main Hole richly document the seismic wavefield at near-field distances. These recordings are generated by near-surface explosions at several PASO stations. Wave packets observed in the borehole from these near-surface shots arrive as SV waves, based on their moveout and polarization. Most of the observed S-wave energy arrives at times between direct P and direct S and is interpreted as P to S conversions at internal discontinuities. Forward waveform modeling of the shots detonated at PASO stations 1 to 2 km from the SAFOD wellhead reveals that for these small explosions the effective source may be described, to first order, as the seismic response to an explosive point source. Wave packets arriving at the time of direct S may require the superposition of an explosive point source and a vertical-dipole source. This complements the inferences based on waveform fitting of near-zero offset shots, which provided evidence of additional secondary source components (e.g., delayed implosion). Such secondary sources would probably support failure of a weak upper crustal rock in response to large local shear and isotropic stresses imparted by the chemical explosion (Sammis, 2002). A 1D (vertically-varying) seismic velocity model accounts approximately for arrival times and moveouts of major seismic phases. However, many details of the observed

wavefields demand 2D or 3D seismic wavefield modeling in order to explain them. Continuing work will focus on: (1) applying 2D and 3D seismic wave-propagation codes to a 3D velocity model of the SAFOD region, and (2) more in-depth analysis of the Pilot Hole recordings of the Hole-Ryberg line in order to better understand the origin of observed S wave energy.

ACKNOWLEDGEMENTS

Data has been provided by Paulsson Geophysical Services Inc. SAFOD is a part of Earthscope, a program funded by the National Science Foundation and carried out in cooperation with the U.S. Geological Survey, the International Continental Scientific Drilling Program, Stanford University, NASA, and other agencies.

REFERENCES

Aki, K. and Richards, P. G. (1980). *Quantitative Seismology*, volume 1. W.H. Freeman and Company, San Francisco.

Bleibinhaus, F., Hole, J. A., Ryberg, T., and Fuis, G. S. (2007). Structure of the California Coast Ranges and San Andreas Fault at SAFOD from seismic waveform inversion and reflection imaging, *J. Geophys. Res*. **112**, B06315, doi:10.1029/2006JB004611.

Bouchon, M. (1981). A simple method to calculate greens functions for elastic layered media, *Bull. Seismol. Soc. Am*. **71**, 959–971.

Brocher, T. M. (2006). Empirical relations between elastic wavespeeds and density in the Earth's crust. *Bull. Seismol. Soc. Am* **95**, 2081–2092.

Chavarria, J. A., Goertz, A., Karrenbach, M., Paulsson, B., Milligan, P., Soutyrine, V., Hardin, A., Dushman, D., and LaFlame, L. (2007). The use of VSP techniques for fault zone characterization: An example from the San Andreas Fault. The Leading Edge, June: 770–776.

Dreger, D. and Woods, B. (2002). Regional distance seismic moment tensors of nuclear explosions. *Tectonophysics*, **356**, 139–156.

Friederich, W. and Dalkolmo, J. (1995). Complete synthetic seismograms for a spherically symmetric earth by a numerical computation of the greens function in the frequency domain, *Geophys. J. Int*. **122**, 537–550.

Gardner, G. H. F., Gardner, L. W., and Gregory, A. R. (1984). Formation velocity and density - The diagnostic basics for stratigraphic traps. *Geophysics* **39**:770–780.

Hole, J. A., Ryberg, T., Fuis, G. S., Bleibinhaus, F., and Sharma, A. K. (2006). Structure of the San Andreas Fault Zone at SAFOD from a seismic refraction survey, *Geophys. Res. Lett*. **33**(7), L07312, doi:10.1029/2005GL025194.

Kuhn, M. J. (1985). A numerical study of Lamb's Problem. *Geophys. Prospect.* **33**, 1103–1137.

McPhee, D., Jachens, R. C., and Wentworth, C. M. (2004). Crustal structure across the San Andreas Fault at the SAFOD site from potential field and geologic studies. *Geophys. Res. Lett*. **31**, L12S03.

Mosse, R. P. (1981). Review of seismic source models for underground nuclear explosions. *Bull. Seismol. Soc. Am*. **71**, 1249–1268.

Oye, V. and Ellsworth, W. L. (2005). Orientation of Three-Component Geophones in the San Andreas Fault Observatory at Depth Pilot Hole, Parkfield, California, *Bull. Seismol. Soc. Am* **95**, 751–758.

Patton, H. and Taylor, S. (2011). The apparent explosion moment: Inferences of volumetric moment due to source medium damage by underground nuclear explosions. *J. Geophys. Res*. **116**, B03310.

Pollitz, F.F., J.L. Rubinstein, and W.L. Ellsworth (2012). Source characterization of near-surface explosions at SAFOD, *Bull. Seismol. Soc. Am*, in press.

Sammis, C. G. (2002). Generation of high-frequency P and S wave energy by rock fracture during a buried explosion: its effect on P/S discriminants at low magnitude, in *Proceedings of the 2010 Monitoring Research Review: Ground-Based Nuclear Explosion Monitoring Technologies*, LA-UR-02-5048, Vol. I, pp. 542–551.

Zhang, H., Thurber, C., and Bedrosian, P. (2009). Joint inversion for Vp, Vs, and Vp/Vs at SAFOD, Parkfield, California. *Geochem. Geophys. Geosyst*. **10**, Q11002, doi:10.1029/2009GC002709.

Zhu, L. and Rivera, L. A. (2002). A note on the dynamic and static displacements from a point source in multilayered media. *Geophys. J. Int.* **148**, 619–627.

Zoback, M. D., Hickman, S., and Ellsworth, W. (2010). Scientific drilling into the San Andreas fault zone, *EOS Trans. AGU* **91**(22):197–199.

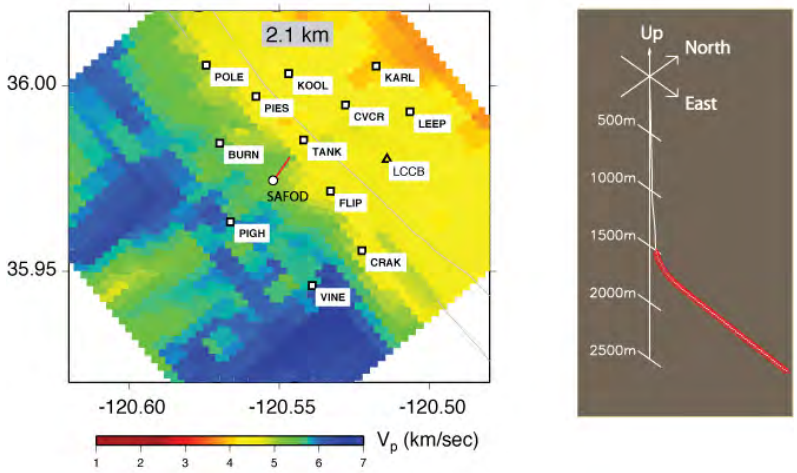

Figure 1. Locations of PASO array stations (squares) and an HRSN station (triangle) for which shots were conducted at recorded at the PGSI downhole seismic array, highlighted in red in the right panel. Superimposed is the V_p structure at 2.1 km depth extracted from Zhang et al. (2009).

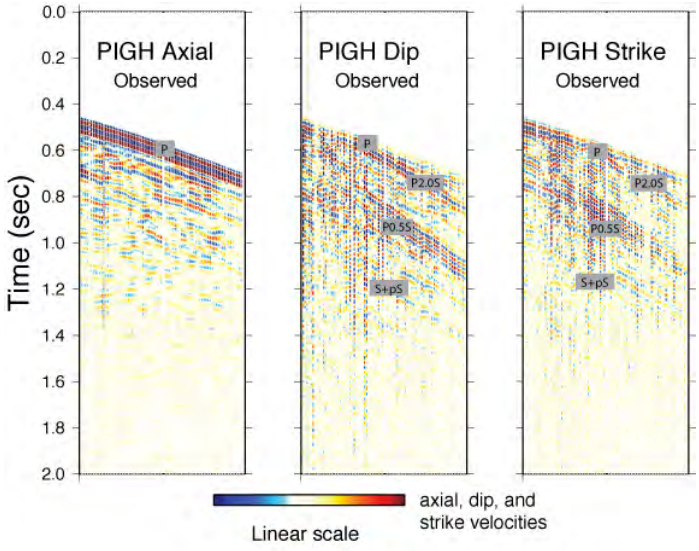

Figure 2. Observed three-component waveforms from the downhole array for a chemical shot located at PASO station PIGH. Seismograms are low-pass filtered at 0.023 s (43.5 Hz).

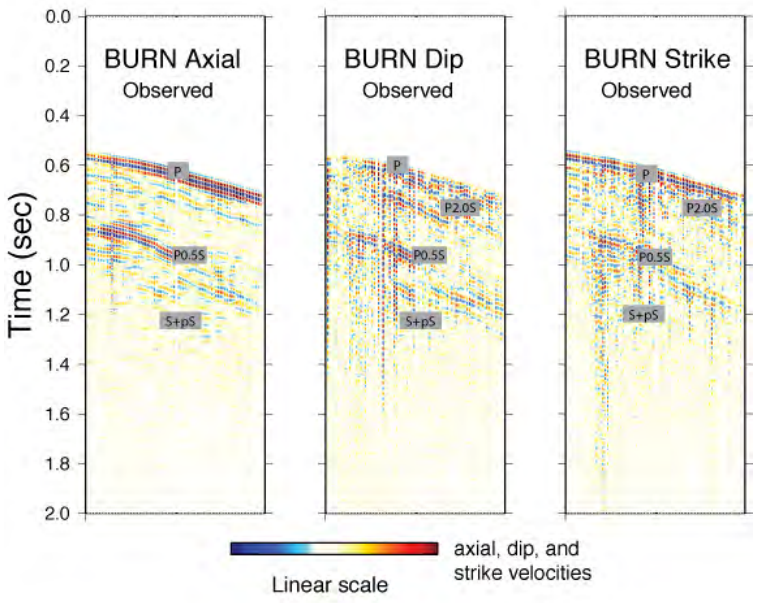

Figure 3. Observed three-component waveforms from the downhole array for a chemical shot located at BURN.

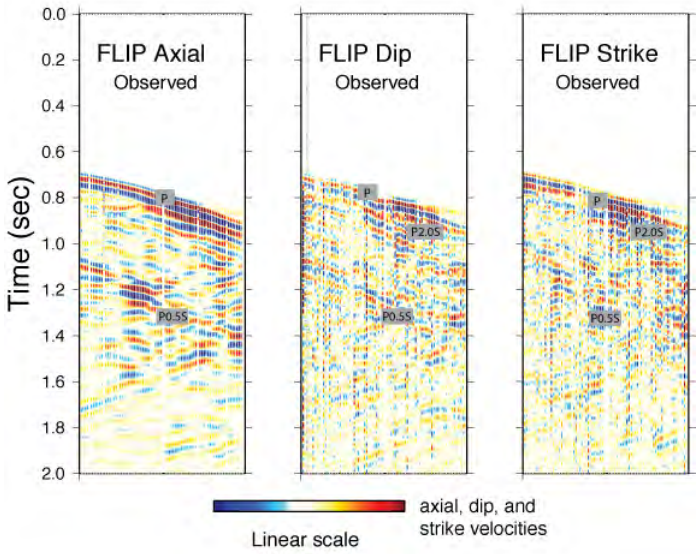

Figure 4. Observed three-component waveforms from the downhole array for a chemical shot located at FLIP. The deep reflections observed in this record likely represent reflections off the San Andreas fault.

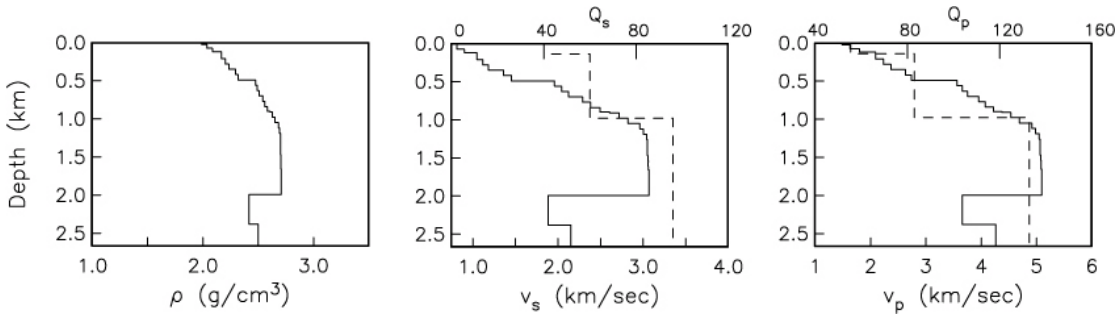

Figure 5. Layered structure of P and S velocities V_p and V_s, density ρ, and P and S-wave quality factors Q_p and Q_s (dashed lines) as a function of depth.

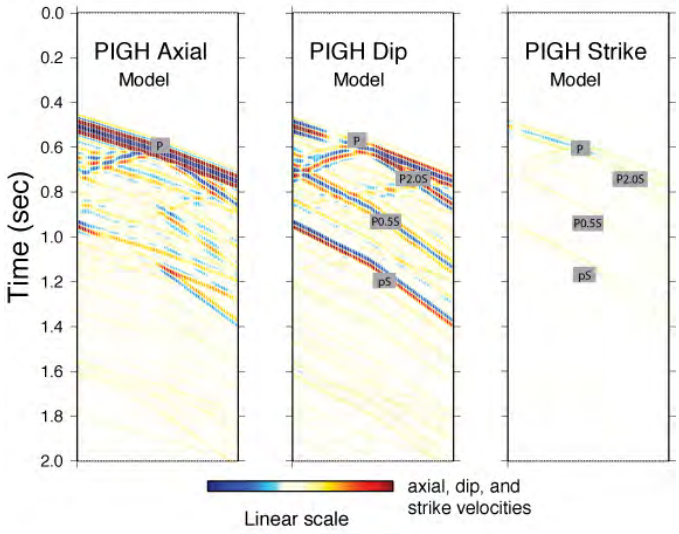

Figure 6. Synthetic wavefield for a shot recorded at the SAFOD downhole array for a shot at PASO station PIGH, using a purely explosive source. P0.5S and P2.0S denote converted P to S waves at strong discontinuities in velocity structure at 0.5 and 2.0 km depth, respectively (Figure 5).

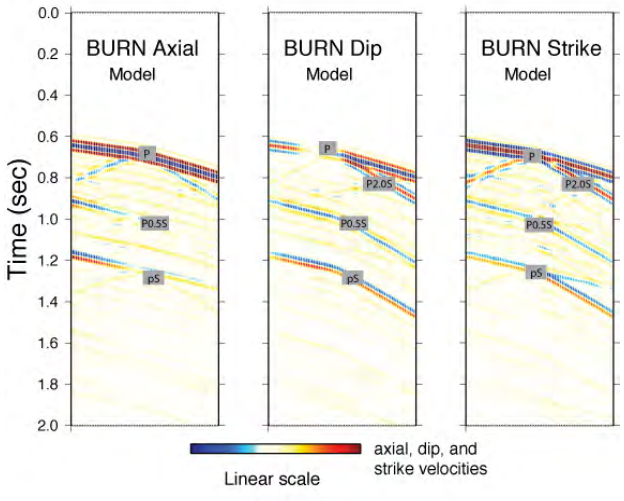

Figure 7. Synthetic wavefield for a shot recorded at the SAFOD downhole array for a shot at PASO station BURN, using a purely explosive source.

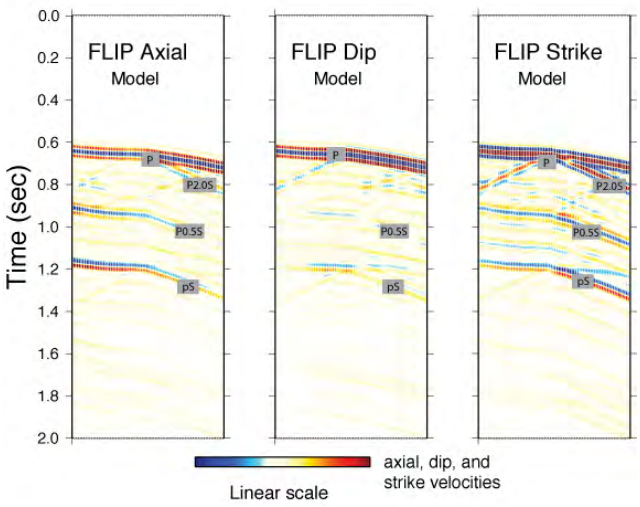

Figure 8. Synthetic wavefield for a shot recorded at the SAFOD downhole array for a shot at PASO station FLIP, using a purely explosive source.

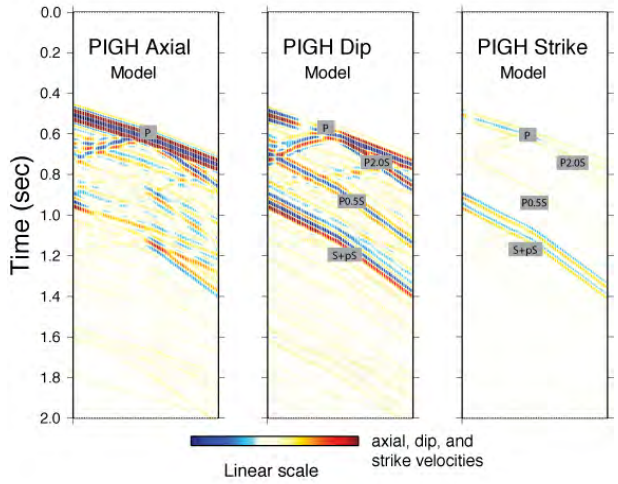

Figure 9. Synthetic wavefield for a shot recorded at the SAFOD downhole array for a shot at PASO station PIGH, using a combined explosive and vertical-dipole source with Md/Mexpl=0.7.

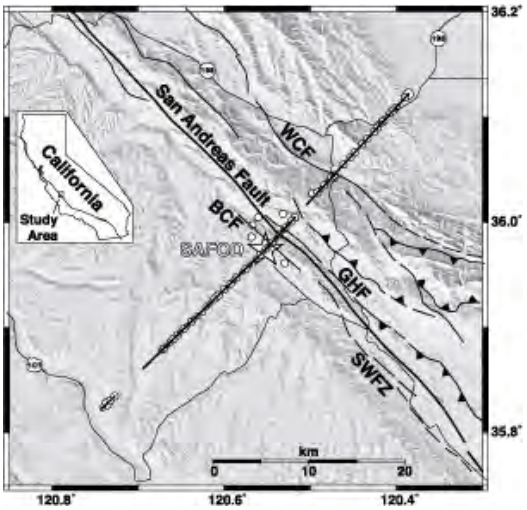

Figure 10. 2003 seismic survey crossing the SAFOD wellhead (Hole-Ryberg Line) superimposed on shaded-relief topography. Shots are shown with white circles. Major faults are BCF, Buzzard Canyon; GHF, Gold Hill; SWFZ, Southwest Fracture Zone; WCF, Waltham Canyon). Modified from Figure 1 of Hole et al. (2006).

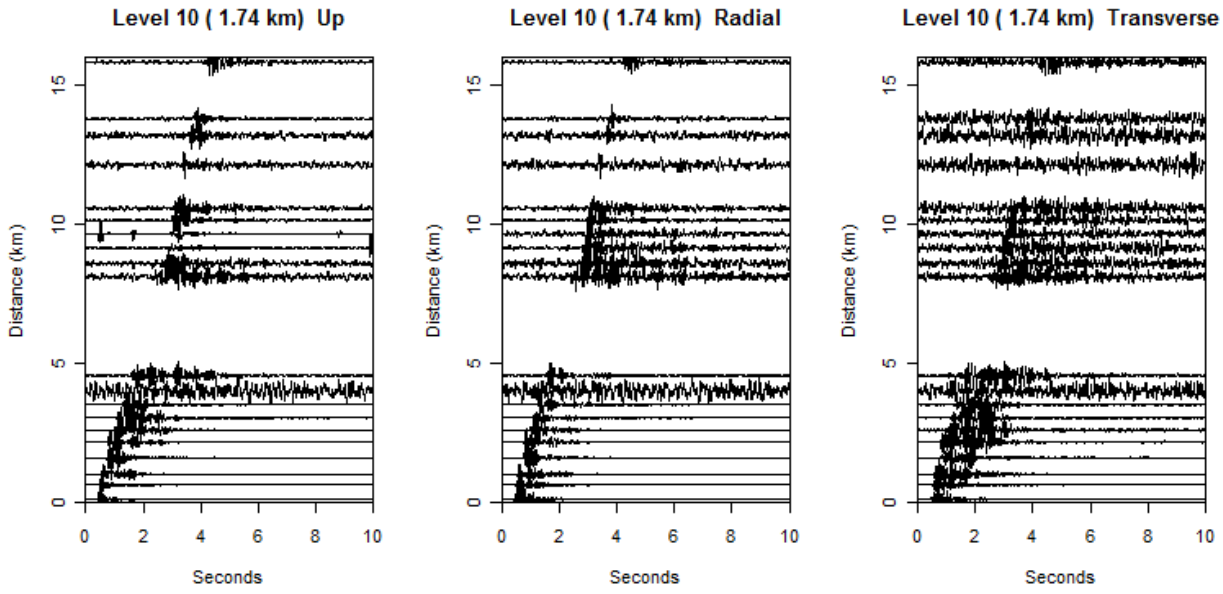

Figure 11. Shot gather at downhole array level 10 (1.74 km) from shots northeast of the Pilot Hole.

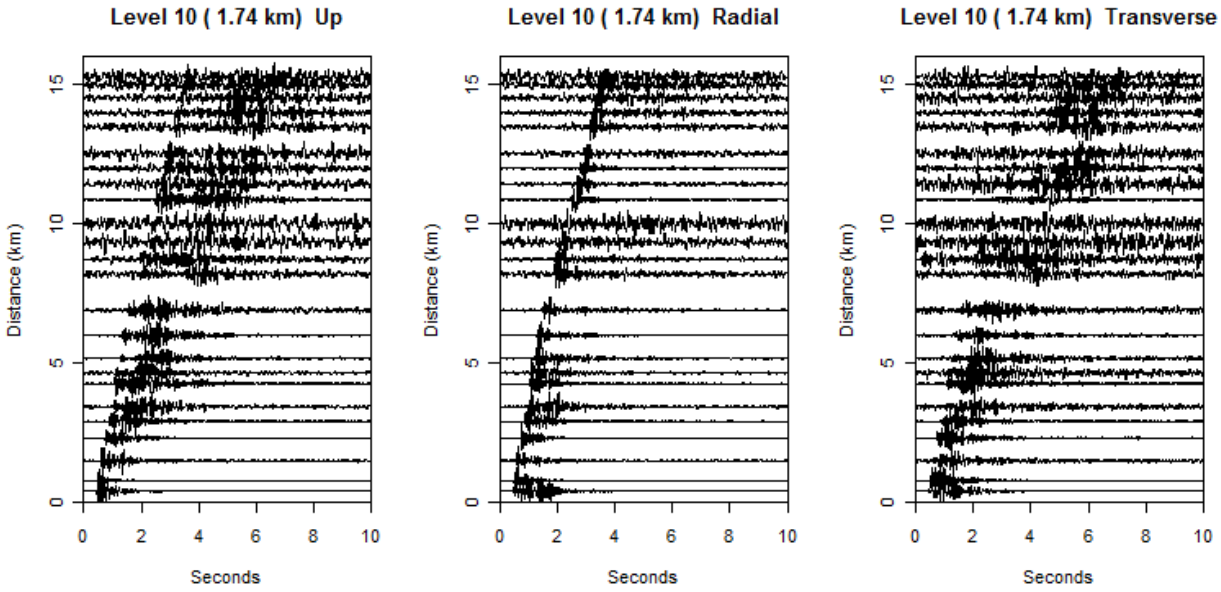

Figure 12. Shot gather at downhole array level 10 (1.74 km) from shots southwest of the Pilot Hole.